JOURNAL OF MATERIALS SCIENCE 26 (1991) 3593 – 3598

Fabrication of $YBa_2Cu_3O_x$ superconductor using Y_2BaCuO_5, $BaCuO_2$ and CuO

KWANGSOO NO, DAE-SHIK CHUNG, JAE-MYUNG KIM, HYE-YOUNG KIM
Department of Materials Science and Engineering, Korea Advanced Institute of Science and Technology, Daejon, Korea

WONBAEK KIM, GUNCHOO SHIM
Korea Institute of Energy and Resources, Daejon, Korea

$YBa_2Cu_3O_x$ superconductor was synthesized using Y_2BaCuO_5, $BaCuO_2$, and CuO powder mixture. Reaction temperatures were identified using differential thermal analysis (DTA) and thermogravimetry (TG) for syntheses of precursor powders and the powder mixtures. Appropriate reaction temperatures for Y_2BaCuO_5 and $BaCuO_2$ precursor powders were 950 and 930 °C, respectively. Two endothermic reactions involving melt formations were identified on the DTA and TG curves of the powder mixture, and the liquid increased the reactivity of the $YBa_2Cu_3O_x$ formation. Powder mixture samples were sintered at various temperatures ranging from 880 to 1000 °C. Microstructural and X-ray powder diffraction studies showed $YBa_2Cu_3O_x$ and impurities to be formed in the samples sintered at various temperatures. The samples sintered at 990 and 1000 °C showed dense microstructures. The critical temperature was 84 K for the sample sintered at 880 °C and rose to 92 K as the sintering temperature increased.

1. Introduction

The standard powder processing technique for preparing $YBa_2Cu_3O_x$ (1 2 3) ceramics consists of mixing powders of Y_2O_3, $BaCO_3$ and CuO followed by solid state reaction at high temperatures. To obtain complete reaction, it is generally necessary to use additional cycles of grinding, pelletizing and reaction. Regional inhomogeneity in the starting powder mixture produces stable minor impurities, it is almost impossible to eliminate those impurities with the additional reaction cycles. There have been many attempts [1] to eliminate the impurities and to improve the density. Hermann and Sheng [2] found a technique for preparing 1 2 3 ceramics consisting of reacting molten Ba–Cu oxide and mixture of 1 2 3 and Y_2BaCuO_5 (2 1 1). The authors claimed that the reaction involving melt forms in their technique provided faster reaction than that involving interatomic diffusion in the solid state reaction technique, and that the technique produced nearly void-free ceramics.

Fig. 1 shows a ternary phase diagram with the solid phases believed to be in equilibrium with 1 2 3 in air [3]. Because 1 2 3 is in equilibrium with 2 1 1, 0 1 1, and 0 0 1, it is possible that 1 2 3 forms by reacting with a powder mixture of those phases by the following reaction at appropriate temperatures.

$$Y_2BaCuO_5 + 3BaCuO_2 + 2CuO \rightarrow 2YBa_2Cu_3O_{6.} + \tfrac{1}{2}O_2\uparrow \quad (1)$$

In the present study, 2 1 1 and 0 1 1 precursor powders were synthesized using solid state reaction, the appropriate temperatures for the fabrication of 1 2 3 ceramics by reacting 2 1 1, 0 1 1, and 0 1 1 powder mixture were investigated, and the temperature effects on the microstructures and superconductivities of the ceramics were analysed.

2. Experimental procedure

Batches of 50 g powder mixture for Y_2BaCuO_5 (2 1 1) and $BaCuO_2$ (0 1 1) precursor powders were made from reagent-grade Y_2O_3, and $BaCO_3$ and CuO powders. Appropriate amounts of powders were mixed and ground in plastic jars with high-density Al_2O_3 balls and ethanol for 24 h. The slurries were dried at 110 °C in an oven overnight, and the dried powder mixtures were ground in an agate mortar and pestle for 1 h. Pellets (10 g) of the powder mixtures were pressed in a 1.9 cm steel mould at 20 MPa. They were then reacted on cleaved single-crystal MgO at 950 °C for 2 1 1 and 930 °C for 0 1 1 for 24 h. After the first reaction, the pellets were ground in an agate mortar and pestle for 30 min and then repelletized for the second reaction using the same procedure as for the first reaction. These pellets were ground in an agate mortar and pestle for 30 min and used as precursor powders to fabricate 1 2 3 ceramics.

A 50 g batch of powder mixture for $YBa_2Cu_3O_x$ (1 2 3) ceramics was made from reacted 2 1 1 and 0 1 1 powders and reagent-grade CuO (0 0 1) powder. Appropriate amounts of powders based on Equation 1 were mixed and ground in an agate mortar and pestle for 6 h. Pellets (2.5 g) of the powder mixture were

0022–2461/91 $03.00 + .12

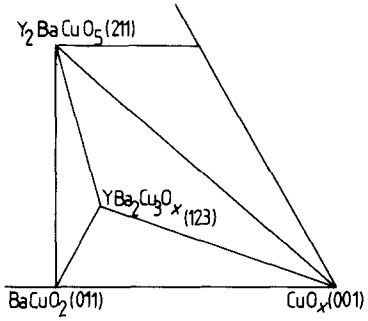

Figure 1 Ternary phase diagram showing the solid phases which are in equilibrium with 1 2 3 [3].

pressed in a 1.9 cm steel mould at 80 MPa and sintered under flowing oxygen at 100 $cm^3 min^{-1}$ on cleaved single-crystal MgO at temperatures varying from 880 to 1000 °C for 24 h, with a final furnace cool to 500 °C, a 5 h hold at 500 °C, and a furnace cool to room temperature.

The appropriate reaction temperatures were investigated using a differential thermal analyser (DTA) and a thermogravimetric (TG) analyser for synthesizing 2 1 1 and 0 1 1 precursor powders from Y_2O_3, $BaCO_3$, and CuO powder mixtures and for synthesizing 1 2 3 ceramics from 2 1 1, 0 1 1, and 0 0 1 powder mixture. After each reaction and grinding, the phases formed during the reactions were identified using X-ray powder diffraction. The densities of the ceramics relative to the theoretical density of 1 2 3 were calculated using weight and dimensions. The microstructure was observed using an optical microscope and a scanning electron microscope (SEM).

The reacted pellets were cut using a diamond saw to obtain specimens of 0.1 cm × 0.2 cm area for resistivity measurements. The superconductivity transition temperatures were measured using d.c. resistivity measurements with a four-point probe method. Four contacts were made using sharp gold pressure contacts, and the temperatures were measured using a diode.

3. Results and discussion

Appropriate reaction temperatures were investigated using DTA and TG for synthesizing 2 1 1 and 0 1 1 precursor powders. Fig. 2 shows DTA and TG curves for the powder mixture consisting of appropriate amounts of Y_2O_3, $BaCO_3$, and CuO for synthesizing 2 1 1. Two endothermic peaks, one beginning at 805 °C and one at 920 °C, were observed on the DTA curve. The peak beginning at 805 °C was also observed on the DTA curve for the powder mixture consisting of appropriate amounts of $BaCO_3$ and CuO for synthesizing 0 1 1, as is shown in Fig. 3. In both figures, TG curves did not show any weight change during the endothermic reaction; this reaction may indicate a phase change during the heating. The endothermic peak beginning at 920 °C showed a maximum at 935 °C, and a weight loss started at 935 °C, as shown on the TG curve in Fig. 2. The weight loss had not ended at 1000 °C, at which temperature heating was stopped in the DTA run. After 1000 °C heating for DTA and TG investigation the resulting pellet was

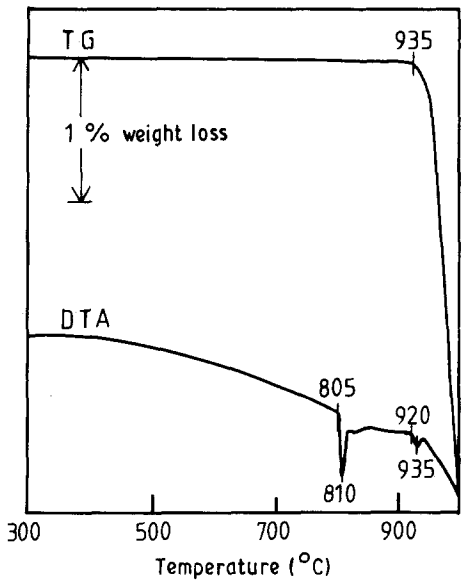

Figure 2 DTA and TG curves for the powder mixture consisting of appropriate amounts of Y_2O_3, $BaCO_3$ and CuO for synthesizing Y_2BaCuO_5.

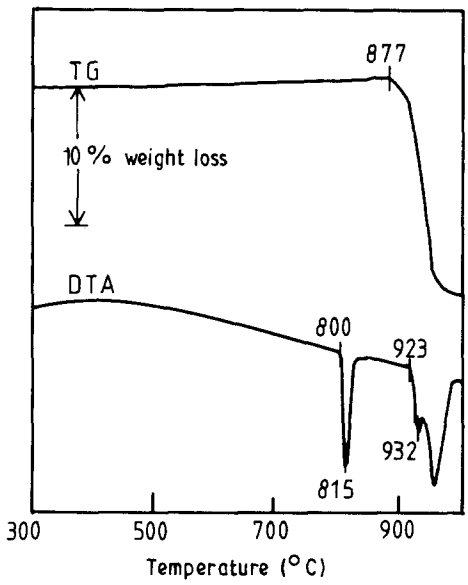

Figure 3 DTA and TG curves for the powder mixture consisting of appropriate amounts of $BaCO_3$ and CuO for synthesizing $BaCuO_2$.

green, and the X-ray powder diffraction pattern of the resulting pellet was well matched to the published pattern of 2 1 1 [4], which indicated that the resulting pellet mainly consisted of 2 1 1. Therefore, a reaction temperature of 950 °C was used for synthesizing 2 1 1 precursor powder. The X-ray powder diffraction pattern is shown in Fig. 4a for 2 1 1 precursor powder synthesized in this study, and the pattern well matches the published pattern of 2 1 1.

Fig. 3 shows DTA and TG curves for the powder mixture consisting of appropriate amounts of $BaCO_3$ and CuO for synthesizing 0 1 1. Three endothermic peaks, one beginning at 800 °C, one at 923 °C, and one at around 940 °C, were observed on the DTA curve. Because the melting point of $BaCuO_2$ has been reported [3, 5] to be over 1000 °C, the endothermic peaks did not represent the melting of $BaCuO_2$. It has been reported that eutectic melting occurs at around 900 °C by the reaction 0 1 1 + 0 0 1 → liquid [3] and

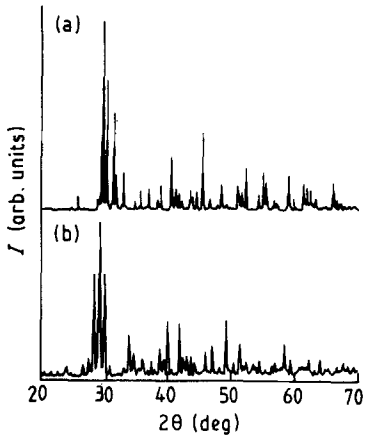

Figure 4 X-ray powder diffraction patterns of (a) Y_2BaCuO_5, and (b) $BaCuO_2$ synthesized in this study.

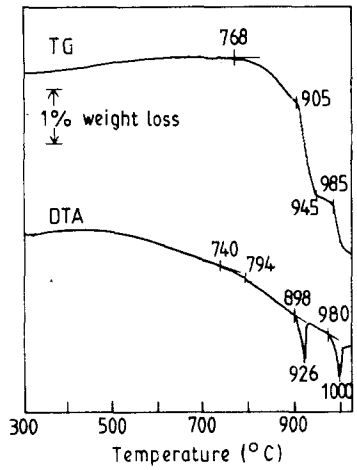

Figure 5 DTA and TG curves for the powder mixture consisting of appropriate amounts of Y_2BaCuO_5, $BaCuO_2$ and CuO for synthesizing $YBa_2Cu_3O_x$.

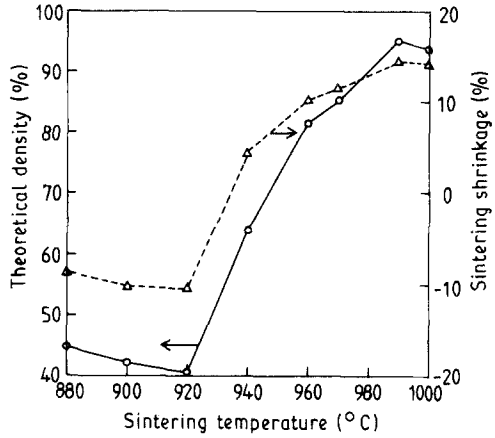

Figure 6 Relationships between sintering temperatures and per cent theoretical density of $YBa_2Cu_3O_x$ (6.4 g cm^{-2}) and sintering shrinkage.

that endothermic peaks were observed on DTA curves at various temperatures ranging from 912 to 929 °C depending on the composition [5]. $BaCO_3$ and CuO react to form $BaCuO_2$ by following reaction

$$BaCO_3 + CuO \rightarrow BaCuO_2 + CO_2\uparrow \quad (2)$$

Reacted $BaCuO_2$ may react with surrounding CuO to form the eutectic melt. Two endothermic peaks at higher temperatures may represent Equation 2 and the eutectic melt. The TG curve in Fig. 3 shows slow and slight weight gain followed by about 15% weight loss beginning at 880 °C. Equation 2 predicts 15.9% weight loss, and the observed weight loss on the TG curve closely matches the prediction. The resulting pellet after 1000 °C heating for DTA and TG investigation was black, and the X-ray powder diffraction pattern of the pellet was well matched to the published pattern of 0 1 1 [4]. Therefore, the reaction temperature for the synthesis of 0 1 1 precursor powder was decided to be 930 °C. The X-ray powder diffraction pattern is shown in Fig. 4b for 0 1 1 precursor powder synthesized in this study, and the pattern is well matched to the published pattern of 0 1 1.

After 2 1 1 and 0 1 1 precursor powders were synthesized, appropriate amounts of 2 1 1, 0 1 1, and 0 0 1 powders based on Reaction 1 were mixed to fabricate 1 2 3. Reactions and weight changes during heating the powder mixture were investigated using DTA and TG, as shown in Fig. 5. Three endothermic peaks, one beginning at 794 °C, one 898 °C, and one at 980 °C, were observed on the DTA curve. The TG curve in Fig. 5 shows slow and slight weight gain (about 0.5% gain compared to the original weight at room temperature) followed by three weight loss regions, one beginning at 768 °C, one at 905 °C, and one at 985 °C. The total weight loss of the three regions was about 3.8% which is much higher than the 0.61% weight loss predicted using Equation 1. This discrepancy between the predicted and the observed losses was no big surprise because the compounds, especially $BaCuO_2$, have been known to be humidity and carbon dioxide absorbing.

In order to understand phase formations in the samples sintered at various temperatures and their superconductivity changes, a powder mixture consisting of appropriate amounts of 2 1 1, 0 1 1, and 0 0 1 based on Reaction 1 was pressed, and the pellets were sintered at temperatures varying from 880 to 1000 °C for 24 h with finally a furnace cool to 500 °C, a 5 h hold at 500 °C, and the furnace cool to room temperature. Fig. 6 shows the per cent theoretical density of $YBa_2Cu_3O_x$ (6.4 g cm^{-2}) and sintering shrinkages of the pellets sintered at various temperatures. The theoretical densities of different samples may vary because some samples consisted of phases other than 1 2 3, but the percentage may give a rough idea of the relative amounts of pores in the samples. The samples sintered at temperatures between 880 and 920 °C had very low densities. The sintering shrinkages of these samples were negative, which indicates that the samples became larger during the sintering process.

Fig. 7a and b show the optical images of the microstructures for the samples sintered at 880 and 900 °C, respectively. The microstructures show unreacted particles which were identified as 2 1 1, 0 1 1 and 0 0 1 by colour differences in the polarized images and by elemental analysis using a scanning electron microscope (SEM) with energy dispersive X-ray spectroscopy (EDXS). Fig. 8a shows the X-ray powder diffraction pattern of the sample sintered at 880 °C. The major peaks match the published peaks well for the

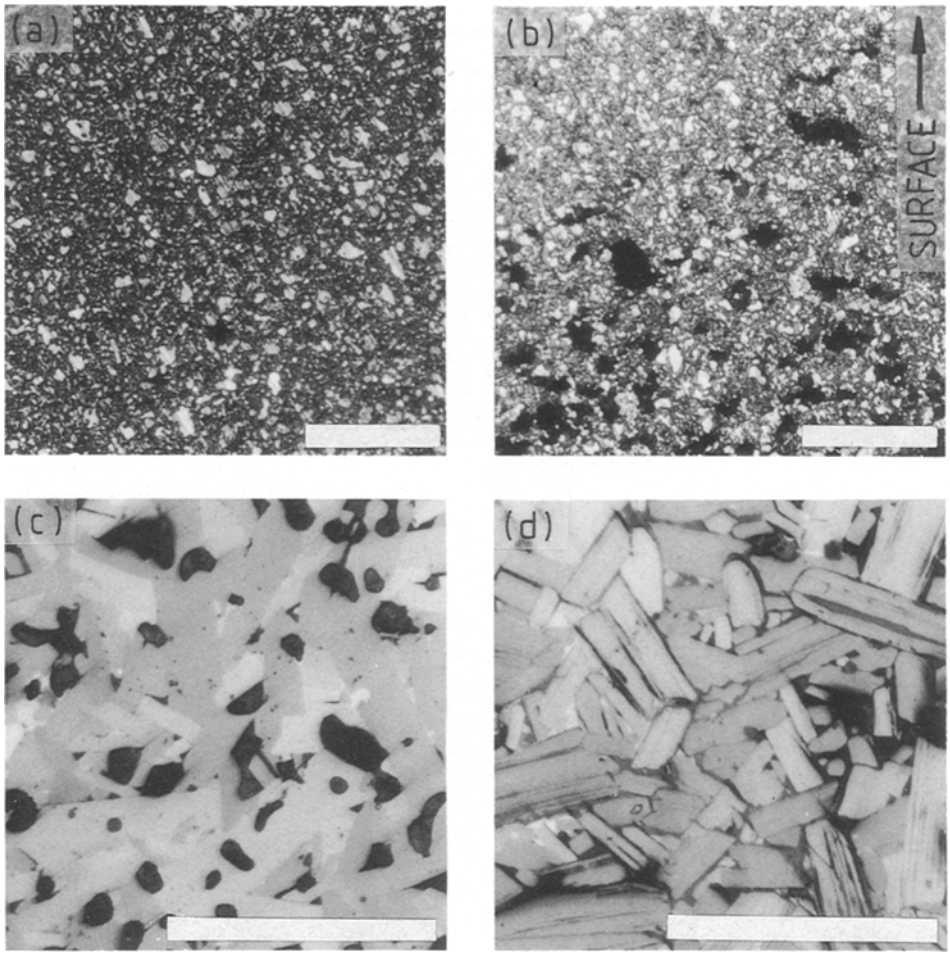

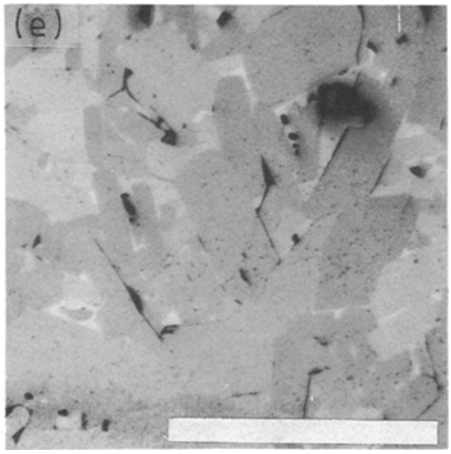

Figure 7 Optical images of the microstructures of the samples sintered at (a) 880 °C, (b) 900 °C, (c) 970 °C, and (d) 990 °C and (e) 1000 °C. Scale bars = 100 μm.

orthorhombic 1 2 3 phase. The peaks representing the 0 1 1 phase, as shown in Fig. 4b, were observed in the pattern, which agrees with observations made in the microstructure study. The relative intensity of the peaks representing the 0 1 1 phase to those representing the 1 2 3 phase decreased as the sintering temperature increased, indicating that the amount of second phases decreased as the sintering temperature increased. Comparing the microstructures of the samples sintered at 880 °C (Fig. 7a) and 900 °C (Fig. 7b), it may be noticed that the microstructure of the sample sintered at 900 °C consisted of large voids trapped inside the sample. These voids were not observed in the microstructure of the sample sintered at 880 °C. The TG curve in Fig. 5 shows a gradual weight loss beginning at 768 °C followed by a steep weight loss beginning at 905 °C, which may correspond to the endothermic reaction beginning at 898 °C on the DTA curve. The eutectic melting occurs at around 900 °C by the reaction $0\,1\,1 + 0\,0\,1 \rightarrow$ liquid [3, 6]. In the sample sintered at 880 °C, 1 2 3 phase was synthesized without the eutectic melt, and Reaction 1 involved only interatomic diffusion at rates which were usually slow at that temperature. Because of the slow gas evolution during the reaction, the sample volume increased, and the density decreased, as shown in Fig. 6. In the samples sintered at temperatures over 900 °C, the eutectic melt was formed; Reaction 1 involving the melt was faster than the reaction involving only interatomic diffusion. Because the sample externally was already densified, the gas evolving inside the sample, could not diffuse through the sample to the outside, was trapped inside the sample, and further increased the sample volume and porosity. From the sample sintered at 940 °C, the per cent theoretical density and the sintering shrinkage were found to increase as the sintering temperature increased up to 990 °C, as shown in Fig. 6.

The light image of the microstructure of the sample sintered at 970 °C (Fig. 7c) shows the typical microstructure of solid-state reacted 1 2 3 ceramics. The microstructure still consists of large voids. Fig. 8b shows the X-ray powder diffraction pattern of the sample sintered at 970 °C. Most peaks are well

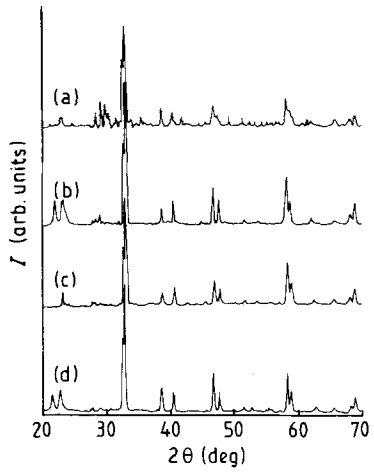

Figure 8 X-ray powder diffraction patterns of the samples sintered at (a) 880 °C, (b) 970 °C, (c) 990 °C, and (d) 1000 °C.

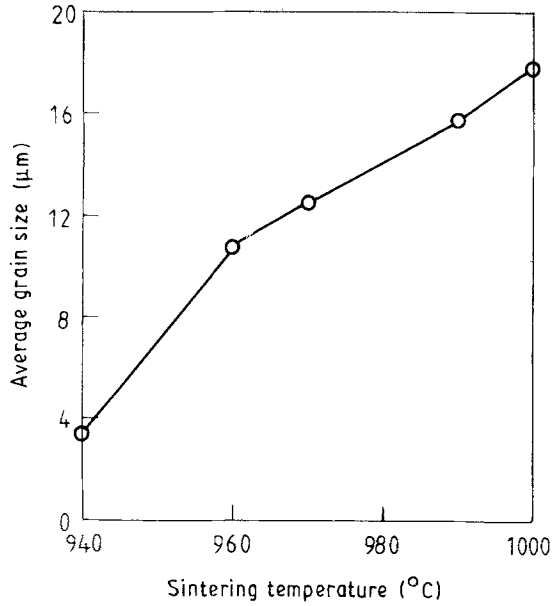

Figure 9 The relationship between the sintering temperature and average grain size.

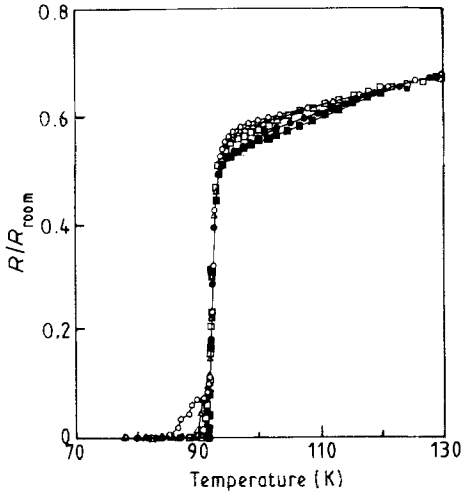

Figure 10 Relative resistance changes upon cooling of the samples sintered at various temperatures: (○) 880, (△) 900, (□) 920, (●) 940, (■) 990 K.

matched to the published peaks for the orthorhombic 1 2 3 phase, and no peak representing impurity was observed within the detection limit of X-ray powder diffraction method.

Fig. 9 shows the relationship between sintering temperature and average grain size. The average grain sizes of the samples sintered at temperatures varying from 880 to 920 °C could not be measured because identification of 1 2 3 grains among the second phases was not possible, but they appeared to be near 1 μm. As the sintering temperature increased, the average grain size increased. The slope of the relation between the average grain size and the sintering temperature is steeper for the temperature range 940 to 960 °C than for the temperature range 960 to 1000 °C, which corresponds to the observations made of the per cent theoretical density and sintering shrinkage relationships.

The light image of the microstructure of the sample sintered at 990 °C (Fig. 7d) shows different features inside the 1 2 3 grains compared to those sintered at lower temperatures (see Fig. 7c as an example) and 1000 °C (Fig. 7e). The features appear to be second phase which has penetrated into the cracks inside the grains. The cracks are usually formed parallel to the long axis of the grain during cooling due to the thermal expansion anisotropy of the 1 2 3 phase. But, because similar cracks were not observed in the microstructure of the sample sintered at 1000 °C (Fig. 7e) with the same cooling rate, cracks consisting of second phase were not formed during cooling but due to a possible liquid penetration along the long axis of the grain, which is known to be the weaker axis in 1 2 3 crystal structure, at the sintering temperature. Semiquantitative elemental analysis using SEM with EDXS showed that the second phase inside the 1 2 3 grains consisted of 0.8:1.7:1:4.1 atomic ratio of Y:Ba:Cu:O. The DTA curve in Fig. 5 shows an endothermic reaction beginning at 980 °C, which may correspond to the liquid formation inside the 1 2 3 grains. Aselage and Keefer [5] indicated that melting occurs at about 970 °C by the peritectic reaction 2 1 1 + 0 1 1 → 2 0 2 + liquid and that melting occurs at about 1000 °C by the eutectic reaction 2 1 1 + 0 1 1 → liquid. According to the elemental analysis data, the endothermic reaction observed in the DTA curve appears to be due to the later eutectic melting. The grains of the sample sintered at 1000 °C did not consist of the second phase internally. This observation may indicate that the formation of the second phase requires time at 990 °C, so that the second phase could not be formed in the sample sintered at 1000 °C. The X-ray diffraction patterns did not show any significant impurity phase for the samples sintered at 990 and 1000 °C, as shown in Fig. 8c and d.

Relative resistance changes upon cooling the samples sintered at various temperatures are shown in Fig. 10. The resistance decreased linearly up to near 130 K. The slopes of the resistance curves increased as the sintering temperature increased from temperatures ranging near 130 to 94 K, at which the resistance dropped rapidly. The sample sintered at 880 °C showed a resistance tail until cooled to 84 K, at which the

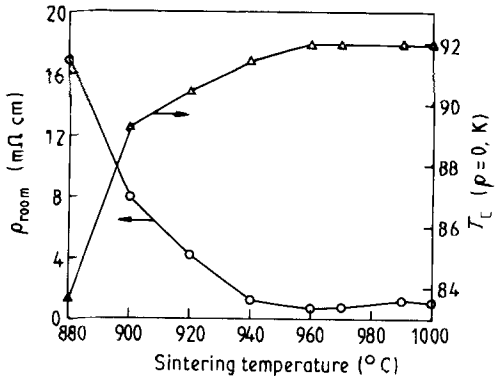

Figure 11 Relationships between the sintering temperature and the room-temperature resistivity and the critical temperature.

resistance was unable to be measured within the resolution of the nanovoltmeter. As the sintering temperature increased, the critical temperature showing immeasurable resistance increased up to 960 °C sintering temperature, above which the critical temperature was 92 K, independent of sintering temperature, as shown in Fig. 11. Fig. 11 also shows the relationship between the room-temperature resistivity and the sintering temperature. The room-temperature resistivity of the sample sintered at 880 °C was around 16.5 mΩcm, and, as the sintering temperature was increased up to 960 °C the room-temperature resistivity decreased; above this temperature the resistivity was around 1 mΩcm. The critical temperature increase and the room-temperature resistivity decrease with sintering temperature were probably due to the decreasing impurity phases and porosity in the sample as the sintering temperature increased, as discussed in preceding sections. The nonsuperconducting impurity phases and porosity decreased the effective area of the current path; consequently, the critical temperature decreased at the current level applied through the sample in this study (1 mA), and the room-temperature resistivity increased because current density decreased.

4. Conclusions

$YBa_2Cu_3O_x$ superconductor was synthesized using Y_2BaCuO_5, $BaCuO_2$ and CuO powder mixture. The appropriate reaction temperatures for Y_2BaCuO_5 and $BaCuO_2$ precursor powders were 950 and 930 °C, respectively. Upon heating Y_2BaCuO_5, $BaCuO_2$ and CuO powder mixture, two endothermic reactions, one beginning at 898 °C and one at 980 °C, were observed. The reactions corresponded to liquid formation and increased the reactivity of $YBa_2Cu_3O_x$ formation. $YBa_2Cu_3O_x$ superconductor was synthesized at a temperature as low as 880 °C. The densities of the samples decreased as the sintering temperatures increased up to 920 °C due to trapped gas inside the samples and increased as the sintering temperatures increased over 940 °C. The samples sintered at temperatures lower than 990 °C consisted of large voids. The samples sintered at 990 and 1000 °C showed near void-free microstructures. The critical temperatures of the samples sintered at temperatures varying from 880 to 940 °C increased as the sintering temperature increased. From 960 to 1000 °C, the critical temperature was 92 K independent of the sintering temperature.

Acknowledgement

This work was sponsored by Korea Science and Engineering Foundation under Contract No. 893-0603-003-2.

References

1. W. J. NELLIS and L. D. WOOLF, *MRS Bull.* **16** (1989) 63.
2. A. M. HERMANN and Z. Z. SHENG, *Appl. Phys. Lett.* **51** (1987) 1854.
3. R. S. ROTH, K. L. DAVIS and J. R. DENNIS, *Adv. Ceram. Mater.* **2** (1987) 303.
4. J. JONES *et al.*, "Synthesis, Chemistry, Electronic Properties, and Magnetism in the Y–Ba–Cu–O Superconductor Systems", in "Chemistry of High-Temperature Superconductors" (American Chemical Society, 1987) pp. A1.
5. T. ASELAGE and K. KEEFER, *J. Mater. Res.* **3** (1989) 1279.
6. B. J. LEE and D. N. LEE, *J. Amer. Ceram. Soc.* **72** (1989) 314.
7. M. NEVRIVA, E. POLLERT, L. MATEJKOVA and A. TRISKA, *J. Crystal Growth* **91** (1988) 434.

Received 20 March
and accepted 24 April 1990